Autologous endothelialisation by the stromal vascular fraction on laminin-bioconjugated nanocellulose-alginate scaffolds

Autologous endothelialisation by the stromal vascular fraction on laminin-bioconjugated nanocellulose–alginate scaffolds

IOP Publishing Biomed. Mater. 18 (2023) 045028 https://doi.org/10.1088/1748-605X/acdebb

Biomedical Materials

OPEN ACCESS

RECEIVED
14 March 2023

REVISED
26 May 2023

ACCEPTED FOR PUBLICATION
15 June 2023

PUBLISHED
26 June 2023

PAPER

Autologous endothelialisation by the stromal vascular fraction on laminin-bioconjugated nanocellulose–alginate scaffolds

Kristin Oskarsdotter[1], Karin Säljö[1,2], Sanna Sämfors[3], Essi M Niemi[4,5,6], Susann Li[7], Stina Simonsson[7], Peter Apelgren[1,2], Hanne Scholz[5,6], Paul Gatenholm[3] and Lars Kölby[1,2,*]

[1] Department of Plastic Surgery, Institute of Clinical Sciences, Sahlgrenska Academy, University of Gothenburg, Gothenburg, Sweden
[2] Department of Plastic Surgery, Region Västra Götaland, Sahlgrenska University Hospital, Gothenburg, Sweden
[3] Department of Chemistry and Chemical Engineering, Chalmers University of Technology, Gothenburg, Sweden
[4] Department of Vascular Surgery, Oslo University Hospital, Oslo, Norway
[5] Institute for Surgical Research, and Department of Transplant Medicine, Oslo University Hospital, Oslo, Norway
[6] Hybrid Technology Hub, Center of Excellence, Institute of Basic Medical Sciences, University of Oslo, Oslo, Norway
[7] Department of Medicinal Chemistry & Cell Biology, Institution of Biomedicine, Sahlgrenska University Hospital, Gothenburg, Sweden
* Author to whom any correspondence should be addressed.

E-mail: lars.kolby@surgery.gu.se

Keywords: autologous endothelialisation, nanocellulose–alginate hydrogels, adipose tissue, sodium periodate oxidation, protein bioconjugation, stromal vascular fraction

Supplementary material for this article is available online

Abstract

Establishing a vascular network in biofabricated tissue grafts is essential for ensuring graft survival. Such networks are dependent on the ability of the scaffold material to facilitate endothelial cell adhesion; however, the clinical translation potential of tissue-engineered scaffolds is hindered by the lack of available autologous sources of vascular cells. Here, we present a novel approach to achieving autologous endothelialisation in nanocellulose-based scaffolds by using adipose tissue-derived vascular cells on nanocellulose-based scaffolds. We used sodium periodate-mediated bioconjugation to covalently bind laminin to the scaffold surface and isolated the stromal vascular fraction and endothelial progenitor cells (EPCs; $CD31^{+}CD45^{-}$) from human lipoaspirate. Additionally, we assessed the adhesive capacity of scaffold bioconjugation *in vitro* using both adipose tissue-derived cell populations and human umbilical vein endothelial cells. The results showed that the bioconjugated scaffold exhibited remarkably higher cell viability and scaffold surface coverage by adhesion regardless of cell type, whereas control groups comprising cells on non-bioconjugated scaffolds exhibited minimal cell adhesion across all cell types. Furthermore, on culture day 3, EPCs seeded on laminin-bioconjugated scaffolds showed positive immunofluorescence staining for the endothelial markers CD31 and CD34, suggesting that the scaffolds promoted progenitor differentiation into mature endothelial cells. These findings present a possible strategy for generating autologous vasculature and thereby increase the clinical relevance of 3D-bioprinted nanocellulose-based constructs.

Abbreviations

3D	three-dimensional
BSA	bovine serum albumin
$CaCl_2$	calcium chloride
DAC	dialdehyde cellulose
DAPI	4′,6-diamidino-2-phenylindole
DPBS	Dulbecco's phosphate-buffered saline
ECGM	endothelial cell growth medium
EPC	endothelial progenitor cell
FACS	fluorescence activated cell sorting
HBSS	Hank's buffered saline solution
HUVEC	human umbilical vein endothelial cell
$NaIO_4$	sodium periodate
SVF	stromal vascular fraction
ToF-SIMS	time-of-flight secondary ion mass spectrometry
VE	vascular endothelial

1. Introduction

In the field of tissue engineering, vascularisation remains a major challenge and bottleneck in the creation of viable, implantable tissues of any larger dimension. A first step in addressing this issue involves achieving recruitment and adhesion of endothelial cells to the tissue-scaffold surface to facilitate endothelialisation. Various biomaterials have been tested for a range of tissue-engineering applications, with nanocellulose showing great potential due to its biocompatibility and tuneable chemical, physical, and mechanical properties [1–8]. As the most abundant biopolymer found in nature, cellulose is also highly accessible, as it can be derived from a wide variety of sources, including plants, bacteria, and tunicates [9]. As a material, it shows significant versatility and application potential, including evaluations for skin and wound healing; artificial vascular grafts; and cartilage-, bone-, and neural-tissue engineering [10].

In recent years, nanocellulose has been successfully used as a bioink for 3D-bioprinting applications, with 3D-bioprinted scaffolds dimensionally stabilised through chemical cross-linking by combining nanocellulose with the polysaccharide alginate, which undergoes sol–gel transition when exposed to divalent cations (e.g. Ca^{2+}) [8, 11–13]. Nanocellulose–alginate bioinks successfully combine their respective advantageous mechanical and rheological properties, particularly the shear-thinning properties of nanocellulose with the cross-linking ability of alginate, to provide 3D constructs that can remain stable under cell culture conditions [14–16]. A major advantage of using nanocellulose in biomedical applications is the limited biomaterial interaction with cells *in vivo* as well as low degree of cell adhesion, preventing the elicitation of a strong inflammatory reaction and foreign body response [7, 17, 18]. However, the same feature becomes disadvantageous considering vascularisation, as the adhesion of endothelial cells on nanocellulose in its unaltered form is difficult [18].

Previous studies attempted to modify cellulose in order to facilitate cell adhesion, with the addition of proteins native to the extracellular matrix (ECM) such as fibronectin and collagen, to scaffolds to promote attachment by mimicking the natural environment of cells representing an attractive approach [18–22]. One method involves the use of readily available hydroxyl groups on the cellulose glucose subunit, any of which can be oxidised to allow reactions with protein amine groups to form covalent bonds between cellulose and the protein. In addition to fibronectin and collagen, laminin is relevant in this context. Previous studies have demonstrated how laminin promotes neovascularization and endothelialisation when immobilized on various synthetic biomaterials such as polytetrafluoroethylene, polyvinyl alcohol and polycaprolactone [23–25]. To this date, there is no study accounting for laminin immobilized on nanocellulose-based hydrogel scaffolds, which could be a viable strategy for endothelialisation of nanocellulose.

Isolation of sufficient amounts of cells of a relevant type remains a major challenge within tissue engineering. Isolation of primary cells directly from patients depends on the general availability and abundance of cells in the tissue of interest [26]. This makes adipose tissue highly relevant in this context, given its easy accessibility, ability to be isolated in abundance by liposuction, and the limited donor discomfort associated with its acquisition. Additionally, the SVF of adipose tissue represents a highly diverse cell population that contains fibroblasts, pericytes, immune cells, vascular cells, mesenchymal stem cells, and various proangiogenic proteins and growth factors [27–29]. This heterogeneity and the accompanying secretome of the cell population make the SVF highly interesting as a cell source for various applications and a vascularisation tool for tissue engineering, given its reported ability to spontaneously assemble into vascular networks [30].

In this study, we evaluated a novel strategy for autologous endothelialisation of nanocellulose-based scaffolds using cells from human adipose tissue (lipoaspirate), including the SVF and EPCs. The findings demonstrated a viable method for promoting cell adhesion on nanocellulose-based hydrogel scaffolds through scaffold functionalisation by $NaIO_4$ oxidation and bioconjugation of laminin as a promotor of cell adhesion. Moreover, this technique could serve as a tool for guiding the development of autologous vasculature within engineered tissues.

2. Material and methods

2.1. Chemicals and materials

All scaffolds were fabricated using 2.5% (w/v; in water) medical-grade tunicate nanocellulose hydrogels (TUNICELL ETC; Ocean TuniCell AS, Norway) and lyophilized sterile sodium alginate powder (Pronova SLG100; DuPont NovaMatrix, Sandvika, Norway) reconstituted in D-mannitol (Sigma-Aldrich, Schnelldorf, Germany). $CaCl_2$ (Sigma-Aldrich) solution was used for all cross-linking activities. Bioconjugation was performed using sodium (meta)periodate ($NaIO_4$), HBSS, and natural mouse laminin (Sigma-Aldrich). Ringer's acetate (Fresenius Kabi, Halden, Norway) was used to wash the harvested adipose tissue. For cell culture, HUVECs, as well as adipose tissue-derived cell populations (the SVF and EPCs), were expanded using ECGM and supplements (PromoCell, Heidelberg, Germany; Lonza Group AG, Basel, Switzerland). All cells were detached using TrypLE solution (Thermo

Fisher Scientific, Waltham, MA, USA) and DPBS (Sigma-Aldrich), and viability was assessed using a LIVE/DEAD cell viability kit (Thermo Fisher Scientific). Cell fixation and permeabilisation were performed using 4% paraformaldehyde (pH 6.9) and Triton X-100 non-ionic detergent (Sigma-Aldrich), with fluorescence imaging performed using ActinRed555 ReadyProbes (rhodamine phalloidin) and NucBlue fixed-cell ReadyProbes reagent (DAPI; Thermo Fisher Scientific). Blocking for immunofluorescence staining was performed using either BSA (Sigma-Aldrich) or donkey serum (MilliporeSigma, Burlington, MA, USA) and the secondary antibodies donkey anti-sheep AlexaFluor488 and donkey anti-rabbit AlexaFluor594 (Thermo Fisher Scientific). Primary antibodies included sheep polyclonal human-specific CD31 (clone hCD31; R&D Systems, Abingdon, UK) and rabbit polyclonal VE-cadherin (Abcam, Cambridge, UK). Fluorescence-labelled antibodies included CD31 (clone WM59, Horizon V500; #563454) and PerCP-Cy5.5-conjugated CD34 (clone 8G12; #347222) (BD Biosciences, Franklin Lakes, NJ, USA). All samples were mounted on coverslips using either Vectashield antifade mounting medium (VectorLabs, Stockholm, Sweden) or Invitrogen SlowFade Gold antifade mounting medium with DAPI (Thermo Fisher Scientific). For FACS, we used the following fluorescence-labelled antibodies: FITC-conjugated CD105 (clone MEM-226; #561443; Thermo Fisher Scientific), PE-conjugated CD73 (clone AD2; #550257; BD Biosciences), PE-Cy7-conjugated CD146 (clone P1H12; #562135; BD Biosciences), APC-conjugated CD90 (clone 5 E10; #559869; BD Biosciences), APC-Cy7-conjugated CD45 (clone 2D1; #348815; BD Biosciences), CD44 (clone G4426, Horizon V450; #561292; BD Biosciences), CD31 (clone WM59, Horizon V500; #563454; BD Biosciences), and PerCP-Cy5.5-conjugated CD34 (clone 8G12; #347222; BD Biosciences). All solutions were sterile-filtered using a 0.1 μm MillexW filter unit (MerckMillipore, Billerica, MA, USA).

2.2. Preparation of the nanocellulose–alginate hydrogel

Lyophilised sodium alginate powder was dissolved in sterile D-mannitol aqueous solution (4.6%, w/v) and stirred at 300 rpm for 3 h to form a transparent alginate hydrogel (3%, w/v). Sterile tunicate nanocellulose hydrogel (2.5%, w/v) and alginate solution were combined in an 80:20 ratio (v/v) by transferring the gels back and forth between two syringes connected by a Luer-lock adapter (CELLINK, Gothenburg, Sweden) until a homogenous hydrogel was obtained.

2.3. Scaffold fabrication

Hydrogel scaffolds were prepared by dispensing nanocellulose–alginate hydrogel in an even layer (∼1 mm thick) in a Petri dish. Sterile acupuncture needles (d = 250 μm) were placed in parallel on the hydrogel surface and gently pressed into the layer using tweezers. The hydrogel layer was cross-linked by submerging in 100 mM $CaCl_2$ solution for 30 min at room temperature (i.e. 20 °C–25 °C). The needles were then removed from the cross-linked hydrogel layer, leaving half-cylindrical indentations on the scaffold surface that introduced an element of curvature, which reportedly facilitates endothelial cell attachment [31]. Circular scaffolds were produced using a sterile biopsy punch (d = 10 mm) and stored in 0.1 M $CaCl_2$ at 4 °C.

2.4. Scaffold oxidation by $NaIO_4$

To evaluate the optimal $NaIO_4$ concentration for oxidising the scaffold without compromising scaffold integrity during cell culture, an oxidation assay was performed during which the scaffolds were treated with $NaIO_4$ at different concentrations. Briefly, the scaffolds were washed in sterile deionised water, with excess moisture removed by blotting with filter paper. Solutions at four different $NaIO_4$ concentrations (0.05, 0.025, 0.01, and 0.005 M) were prepared by dissolving sodium (meta)periodate powder in deionised water. A portion (100 μl) of each solution was then applied to the blotted scaffolds in the dark, and oxidation was allowed to occur at room temperature, with sampling performed in triplicate after 1 h, 2 h, and 3 h. The reaction was terminated by repeatedly rinsing with deionised water. The oxidised scaffolds were incubated for 24 h in ECGM at 37 °C under 5% CO_2 and 95% relative humidity, after which they were optically and manually evaluated for their structural integrity as a function of $NaIO_4$ concentration and reaction time.

2.5. Laminin bioconjugation to the scaffold surface

Laminin solution was prepared by diluting 1 mg ml^{-1} of natural mouse laminin solution in HBSS to obtain a 100 μg ml^{-1} solution. Scaffold oxidation was performed (as described in section 2.4) using 0.025 M $NaIO_4$ for 1 h. Oxidised scaffolds were rinsed repeatedly in HBSS, blotted dry with filter paper, and then treated with 100 μl of laminin solution. Treated scaffolds were then incubated at 37 °C under 5% CO_2 and 95% relative humidity for 24 h to facilitate bioconjugation. After incubation, excess protein solution was removed by aspiration, followed by repeated rinsing with HBSS.

2.6. ToF-SIMS analysis

To verify bioconjugation and evaluate the effects of elevated $NaIO_4$ concentration and oxidation time on the amount of bound protein, laminin-treated scaffolds were analysed by ToF-SIMS, with the presence of amino acids used to confirm amounts of bound protein. Scaffolds were treated with $NaIO_4$ according

to the protocol described in section 2.4 at concentrations of 0.025 M and 0.05 M, respectively, for 1 h or 2 h, followed by bioconjugation (as described in section 2.5). After bioconjugation, the scaffolds were repeatedly washed with deionised water and dried on an aluminium sheet at 37 °C overnight. The dried scaffolds were analysed using untreated scaffolds as negative controls. ToF-SIMS analysis was performed using a J105 3D chemical imager (Ionoptika Ltd, Eastleigh, UK) designed for the analysis of biological samples [32, 33]. The J105 uses a quasi-continuous primary ion beam and a buncher that focuses the secondary ions before injection into a reflectron ToF analyser. The mass spectra were acquired using a 40 keV gas cluster ion beam of CO_2 with an approximate gas cluster size of 6000. The primary ion current measured into a Faraday cup was 13 pA. From the mass spectra, the intensities of peaks assigned to the immonium ion of different amino acids according to the Mascot database were cumulated, and relative signal intensity as a function of treatment was compared between groups [34]. Depth analysis was performed over an area of 300 $\mu m^2 \times 300\ \mu m^2$ for 32 layers, with an accumulated primary ion-dose density of 1.5×10^{13} ions cm^{-2}. All analyses were performed in positive-ion mode.

2.7. Mechanical analysis by nanoindentation

The effects of bioconjugation on the mechanical properties of the scaffold were evaluated by measuring stiffness by nanoindentation. Because scaffold stiffness is an important factor in the adhesion and functionality of endothelial cells, it is relevant to determine changes in this property following bioconjugation [35]. Scaffolds were treated with 0.025 M $NaIO_4$ for 1 h, followed by laminin bioconjugation for 24 h at 37 °C. After treatment, the bioconjugated samples were stored in HBSS. Nanoindentation was performed using a PIUMA nanoindenter (Optics11 Life, Amsterdam, Netherlands). The samples were mounted in a glass Petri dish using a small drop of tissue glue and covered with HBSS. The indentations were performed at room temperature using a probe with a tip radius of 8.5 μm and a stiffness of 54.3 N m^{-1}. All measurements were performed in indentation mode with an indentation depth of 1 μm. The data were fitted according to a Hertz model, with the effective Young's modulus (E_{eff}) of the samples subsequently calculated.

2.8. Evaluating the effects of bioconjugation on cell adhesion

2.8.1. HUVEC culture

Primary HUVECs were cultured using ECGM (PromoCell, Heidelberg, Germany). Briefly, 25 ml of medium was transferred to a 150 cm^2 vented cell culture flask and incubated at 37 °C under 5% CO_2 and 95% relative humidity for 30 min. One vial containing cryogenically preserved HUVECs (1×10^6 cells) at passage three was quickly thawed in a 37 °C water bath, transferred by pipette to the cell culture flask, and placed in an incubator at 37 °C under 5% CO_2 and 95% relative humidity. The medium was changed every 2 d, and the cells were cultured until reaching 80% confluence, after which they were split.

2.8.2. Cell seeding on the bioconjugated scaffolds

Bioconjugated scaffolds were prepared by treatment with 0.025 M $NaIO_4$ for 1 h, followed by the addition of 100 μg ml^{-1} of natural mouse laminin for 24 h (as described in sections 2.4 and 2.5). Treated scaffolds and untreated controls were placed in a 48-well plate, covered with 300 ml ECGM, and incubated at 37 °C under 5% CO_2 and 95% relative humidity for 30 min. HUVECs at passages four through six were detached by trypsinisation. After aspiration of the medium from the incubated scaffolds, 100 μl of cell suspension was seeded onto the surface at a cell density of 9×10^5 cells cm^{-2}. The cell-laden scaffolds were incubated overnight at 37 °C under 5% CO_2 and 95% relative humidity to allow cell attachment prior to adding 500 ml of fresh ECGM per well. Cells were maintained in static culture for 1 week (the day of seeding was denoted as day 0), with the medium changed every 2 d. For each treatment, samples were collected in triplicate at days 1, 3, and 7 post-seeding.

2.8.3. Viability assay

Assay of HUVEC viability on the bioconjugated scaffolds was performed using a LIVE/DEAD cell viability kit. Briefly, cell medium was aspirated, and scaffolds were washed with HBSS and incubated at 37 °C for 15 min. LIVE/DEAD stain was prepared by mixing calcein-AM and ethidium homodimer-1 at a 1:1 ratio (v/v) and diluting with HBSS. The stain (150 μl) was applied to each scaffold and incubated for 15 min at 37 °C, after which they were washed twice in HBSS for 15 min at 37 °C to remove excess dye. Cells were imaged at 10× using an Olympus TH4-100 fluorescence microscope (Olympus, Hamburg, Germany). Viable cells were imaged by excitation at 488 nm and dead cells at 570 nm. Images were further processed using ImageJ software (National Institutes of Health, Bethesda, MD, USA) to reduce background fluorescence and create composite images enabling visualisation of live and dead cells on each scaffold.

2.8.4. Confocal imaging

To study HUVEC morphology and overall surface coverage on the bioconjugated scaffolds, cell-laden scaffolds prepared and cultured for 1, 3 and 7 d were stained with DAPI and rhodamine–phalloidin to allow imaging of nuclei and actin filaments and study by confocal microscopy. Sample preparation was performed by washing the scaffolds twice with HBSS and fixation in 4% paraformaldehyde supplemented with 20 mM $CaCl_2$ for 20 min at room

temperature. Scaffolds were then rinsed twice with HBSS and permeabilised in 0.1% Triton X-100 in HBSS for 30 min. After rinsing twice with HBSS, actin filaments were stained by adding two drops of ActinRed555 ReadyProbes to each well for 30 min at room temperature. After rinsing with HBSS, cell nuclei were stained using NucBlue fixed-cell ReadyProbes for 5 min at room temperature. Washed and stained scaffolds were mounted on a glass slide with a coverslip using Vectashield antifade mounting medium. Cells were imaged using an LSM 710 NLO upright confocal microscope and ZEN Blue software (Zeiss, Oberkochen, Germany).

Immunofluorescence staining was performed to evaluate the expression of the endothelial cell marker CD31 and VE-cadherin. Cell-laden scaffolds at days 3 and 7 post-seeding were fixed, and nonspecific sites were blocked using 1.5% donkey serum in DPBS for 1 h. All solutions were supplemented with 20 mM $CaCl_2$ to maintain scaffold integrity. Scaffolds were incubated with sheep polyclonal anti-human CD31 (5 μg ml^{-1}) and rabbit polyclonal VE-cadherin (1:300) overnight at 4 °C. Scaffolds were then washed with PBS and incubated for 2 h at room temperature with secondary antibodies (donkey anti-sheep AlexaFluor488 (1:800) and donkey anti-rabbit AlexaFluor594 (1:800)) diluted in 1.5% donkey serum in PBS. The scaffolds were washed in PBS and mounted on a glass coverslip with SlowFade Gold antifade mounting medium with DAPI for nuclear counterstaining. The samples were then imaged with an Axio Observer inverted microscope (Zeiss) and ZEN Blue software using *z*-stacks (6–12 μm slice steps).

2.9. Autologous endothelialisation

2.9.1. Ethical approval

Human adipose tissue was harvested from a healthy donor using power-assisted liposuction and Klein's tumescent solution. The tissue was used in this study after approval from the Regional Ethics Committee of Gothenburg (Dnr: 624-16) and receiving written informed consent for the donor(s). All collected tissue samples were deidentified after donation. All experiments were performed in accordance with the declaration of Helsinki as well as current national guidelines and regulations.

2.9.2. Isolation of the SVF and EPCs

The harvested lipoaspirate was processed using a Celution automated closed system (Cytori Therapeutics, Austin, TX, USA) for extraction of the SVF. The tissue was transferred to the accompanying sterile disposable container and then to the closed processing canister, where it was washed with 37 °C Ringer acetate, weighed, and treated with Celase enzymatic reagent under mechanical agitation. After digestion, the concentrated SVF suspension (5 ml) was extracted using a sterile syringe. Viability and cell number were evaluated using a NucleoCounter NC-200 system (ChemoMetech, Allerod, Denmark).

2.9.3. FACS

To further separate and characterize the SVF, cells were sorted by flow cytometry using the following anti-human monoclonal antibodies: anti-CD105, -CD73, -CD34, -CD146, -CD90, -CD45, -CD44, and -CD31 (BD Biosciences, Franklin Lakes, NJ, USA; Thermo Fisher Scientific, Waltham, MA, USA). Flow cytometric analysis was performed using the FACSAria IIu cell sorter system with FACSDiva software (BD Biosciences). Instrument parameter settings, as well as cytometer setup and tracking runs, were performed according to manufacturer guidelines prior to analysis. The SVF was characterized based on composition with respect to the cell types and EPCs ($CD34^+CD45^-$) isolated from the SVF by FACS. After sorting, the SVF and EPCs were cultured at a seeding density of 5700 cells cm^{-2} in ECGM for 2 weeks (as described in section 2.8.1).

2.9.4. Adipose tissue-derived cell seeding on bioconjugated scaffolds

Unsorted SVF and EPCs cultured for 2 weeks, respectively, were seeded on bioconjugated scaffolds, as described in section 2.8.2 ($n = 7$ scaffolds/group), with HUVEC-laden bioconjugated scaffolds used as a positive control, and untreated scaffolds used as a negative control for all groups. Cells were cultured for 3 d (the day of seeding was denoted as day 0), and cell viability was assessed by LIVE/DEAD assay (as described in section 2.8.2).

2.9.5. Confocal imaging of cell-laden scaffolds

Fixation, permeabilisation, and staining of nuclei (DAPI) and the cytoskeleton (rhodamine–phalloidin) were performed on SVF-, EPC-, and HUVEC-laden bioconjugated constructs. Additionally, immunofluorescence staining was performed using fluorescence-conjugated anti-human antibodies CD31 (5 μl) and CD34 (20 μl), as described in section 2.8.3, except for the use of 1% (w/v) BSA instead of the blocking solution. Stained cells were imaged using an IN Cell Analyzer 6000 confocal microscope (GE Healthcare, Pittsburgh, PA, USA) to analyse both cell-surface coverage and morphology.

2.9.6. Statistical analysis

The total number of cell nuclei were quantified using ImageJ software for image analysis. Statistical analysis was performed to assess and compare cell densities between groups. Significant differences between cell types were calculated using a Kruskal–Wallis test,

whereas differences in cell density between treated and control surfaces were calculated using a Mann–Whitney U test. All calculations were performed using Excel (v.2108; Microsoft Corp., Redmond, WA, USA), with a $p \leqslant 0.05$ was considered significant.

3. Results and discussion

3.1. Scaffold design and oxidation assays

Oxidation assays showed that a range of $NaIO_4$ concentrations demonstrated negligible effects on scaffold integrity, as all replicates remained structurally intact for up to 3 h during oxidation. However, oxidation of the scaffolds in the presence of 0.025 M $NaIO_4$ resulted in signs of disintegration after 2 h, whereas total solid-to-gel transition occurred after 1 h at 0.050 M $NaIO_4$ for all replicates (figure 1). At an oxidation time >1 h at 0.050 M $NaIO_4$, we observed complete scaffold disintegration prior to incubation in cell medium. Although the highest level of oxidation would most likely be achieved at the highest $NaIO_4$ concentration and oxidation time, this result suggested this as impractical, given the disintegrated state of the scaffolds under these conditions. These findings identified the optimal condition as oxidation in the presence of 0.025 M for 1 h to preserve scaffold integrity.

Although nanocellulose oxidation by $NaIO_4$ is not the only option for generating reactive groups for bioconjugation, use of other oxidising agents, including (2,2,6,6-tetramethylpiperidin-1-yl)oxy, ozone, and hypochlorite, mainly target amorphous regions of the cellulose material and potentially lead to heterogeneous results [36, 37]. $NaIO_4$ mainly targets crystalline regions within the cellulose, and $NaIO_4$ oxidation is highly specific, in that it cleaves the C2–C3 bond of the glucose subunit. This results in the formation of two aldehyde groups per unit and conversion of cellulose to DAC and subsequent immobilisation of proteins by the formation of stable covalent bonds between aldehydes and amine groups [38, 39]. Given that this treatment can be conducted under relatively mild conditions without compromising cellulose morphology, $NaIO_4$ oxidation presents a significant advantage for bioconjugation [40, 41]. Additionally, using $NaIO_4$ on cross-linked scaffolds subjects alginate to oxidation, which emphasizes the need to optimize this treatment to ensure the retention of scaffold cross-linking (figure 1(A)). Depending on the application, it might be beneficial to avoid subjecting the alginate to oxidation altogether, as partial oxidation by $NaIO_4$ reportedly accelerates alginate degradation *in vitro* [42]. One approach to possibly adapting this method to avoid alginate exposure to oxidation is to perform this activity prior to hydrogel preparation (i.e. bulk oxidation of the nanocellulose fibrils rather than the cross-linked nanocellulose–alginate scaffolds) in order to generate DAC without compromising scaffold integrity.

3.2. ToF-SIMS analysis of protein bioconjugation

ToF-SIMS analysis revealed several peaks characteristic to amino acids on the bioconjugated scaffolds in the mass spectra (figure S1). The presence of these peaks confirmed successful bioconjugation, given that the untreated controls demonstrated ∼1000-fold lower respective signal intensities for the same peaks. Additionally, the cumulative signal intensities for these peaks at layers 1, 2, and 20 were higher for scaffolds treated with 0.050 M $NaIO_4$ than those with 0.025 M (figure 2(A)). This was not surprising, given that the oxidation level and thus scaffold aldehyde content would logically be higher as a result of the higher $NaIO_4$ concentration and, therefore, create more available binding sites for proteins at the scaffold surface. Although the higher $NaIO_4$ concentration produced a higher signal intensity, both groups demonstrated cumulative signal intensities within the same range (1×10^4).

Depth profiling of the relative signal intensity for m/z 70 (a mass-to-charge ratio associated with several different amino acids) revealed similar profiles for the bioconjugated groups and a consistently low signal intensity for untreated samples. Signal intensity as a function of scaffold layer showed a rapid decline along with increasing layers, confirming that the protein content was significantly associated with the scaffold surface (figure 2(B)). Despite the apparently higher amount of conjugated protein on scaffolds treated with a higher $NaIO_4$ concentration, the oxidation assay demonstrated that this treatment was not practically feasible due to the loss of structural integrity (figure 1(A)). Because we detected comparable amounts of protein on samples treated with a lower $NaIO_4$ concentration and showing retained scaffold structure, this demonstrated 0.025 M $NaIO_4$ as a suitable treatment for bioconjugation.

In this study, we used NaIO4-mediated bioconjugation to enhance cell adhesion via immobilisation of laminin as a constituent of the ECM, facilitator of cell adhesion according to its role as a ligand for integrins in the cell membrane, and inducer of their organisation into tube-like structures [43, 44]. $NaIO_4$-mediated bioconjugation has been used to create biodegradable bacterial cellulose materials, as well as for immobilizing proteins and antibodies onto cellulose hydrogels. Furthermore, such immobilisation is compatible with retained enzyme function and an important factor in preserving the bioactivity of an immobilised protein [39, 44–46]. The results demonstrated the successful $NaIO_4$-mediated bioconjugation of laminin onto nanocellulose–alginate scaffolds and its likely retention of function post-conjugation.

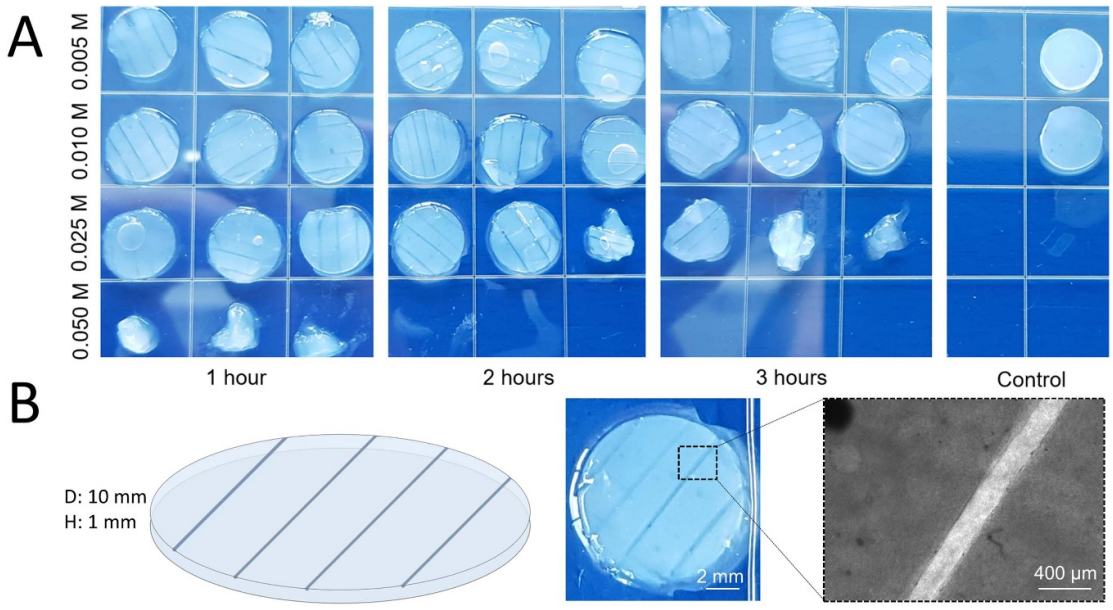

Figure 1. Oxidation of cross-linked nanocellulose–alginate scaffolds. Oxidation of cross-linked scaffolds was performed using various $NaIO_4$ concentrations (0.005, 0.01, 0.025, and 0.05 M) for 1 h, 2 h, and 3 h, respectively, followed by incubation in ECGM for 24 h. Control samples represented un-oxidized nanocellulose–alginate scaffolds. The treatment generating the highest degree of oxidation (i.e. the highest $NaIO_4$ concentration and longest reaction time) at which all replicates retained structural integrity was defined as optimal (identified as 0.025 M $NaIO_4$ for 1 h) (A). Schematic illustration and final scaffold after cross-linking with $CaCl_2$ according to brightfield imaging (4× magnification) of the half-cylindrical indentations (B).

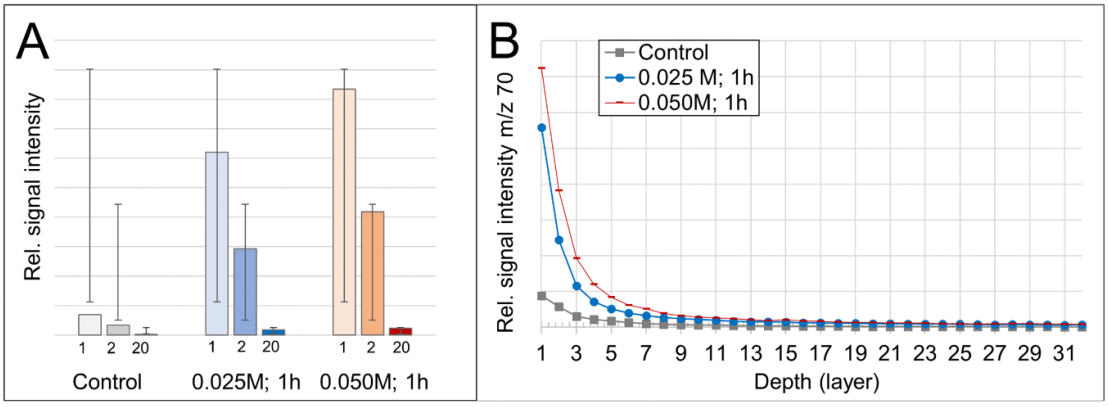

Figure 2. ToF-SIMS analysis of oxidised and bioconjugated nanocellulose–alginate hydrogels. Bar graph showing the cumulative relative signal intensities of the peaks for major amino acids (*m*/*z* 70, *m*/*z* 86, *m*/*z* 110, *m*/*z* 120, *m*/*z* 136, and *m*/*z* 159) for layers 1, 2, and 20 detected on control (untreated scaffolds) and scaffolds oxidised with 0.025 M $NaIO_4$ and 0.05 M $NaIO_4$ for 1 h, respectively. Error bars represent standard deviations ($n = 3$) (A). Depth profile showing the signal intensity of *m*/*z* 70 (amino acid peak) as a function of layer depth in the material (C). Bioconjugation of proteins to the surface was successful after oxidation using both 0.025 M and 0.05 M for 1 h, with no difference in depth observed according to increased $NaIO_4$ concentration.

3.3. Mechanical properties of the bioconjugated scaffolds

Figure 3(A) shows scaffold stiffness as a function of treatment, with similar stiffness levels observed for all three treatment profiles. We observed a slight decrease in surface stiffness in the oxidised group, which was likely a consequence of partial surface degradation caused by broken covalent bonds within both the nanocellulose and the alginate. However, this decreasing trend in stiffness was counteracted by the effects of laminin bioconjugation, which promoted reacquisition of stiffness to levels comparable with those observed in the control group.

Despite the changes in stiffness resulting from treatment, there was no statistical difference between groups. Because scaffold stiffness influences endothelial cell behaviour, we speculated that any positive impact on endothelial cell adhesion as a result of bioconjugation would be attributable to the bioconjugation protocol and not the altered mechanical properties of the scaffold.

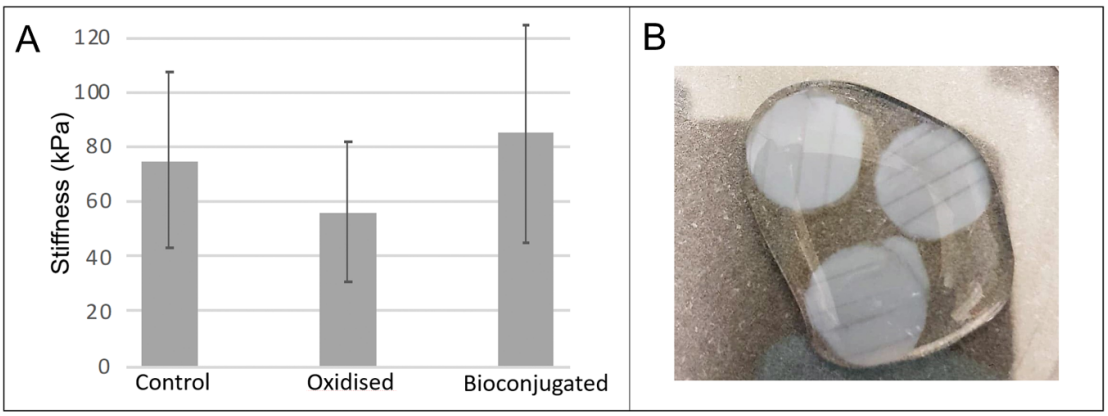

Figure 3. Mechanical properties of oxidised and protein coated nanocellulose–alginate hydrogels measured using a nanoindenter. (A) Stiffness was measured for untreated scaffolds, scaffolds oxidised with 0.025 M $NaIO_4$ for 1 h and bioconjugated scaffolds oxidised with 0.025 M $NaIO_4$ for 1 h followed by laminin bioconjugation for 24 h. Three samples for each group were measured, and three indentations per sample was performed. Error bars show standard deviation. (B) Examples of three untreated control scaffolds in 100 mM $CaCl_2$.

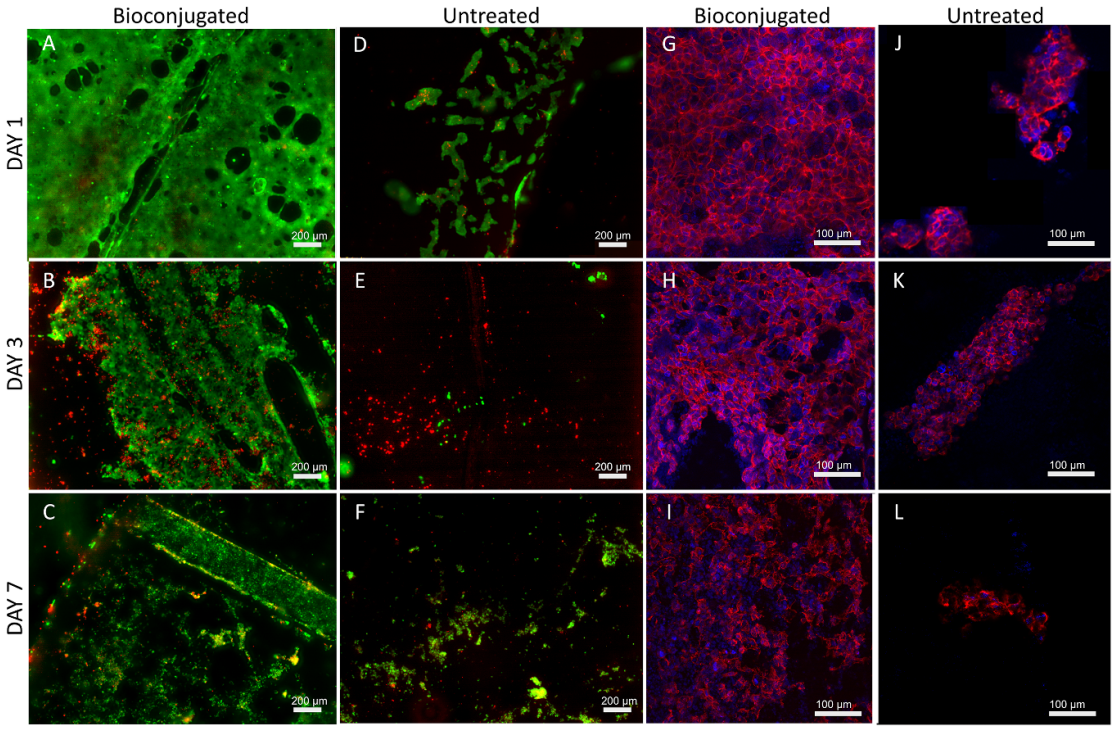

Figure 4. Viability assay and confocal imaging of HUVECs on half-channel nanocellulose–alginate scaffolds. Viability was assessed using LIVE/DEAD staining of cells cultured on bioconjugated scaffolds (0.025 M $NaIO_4$/1 h; 100 µg ml^{-1} laminin/24 h) (A)–(C) or untreated scaffolds (D)–(F) for 1, 3 and 7 d in static culture. Coverage of cells cultured on bioconjugated (G)–(I) and untreated (J)–(L) scaffolds for 1, 3 and 7 d was assessed by confocal microscopy imaging of cell actin filaments (red) with nuclei counterstaining (blue). Analysis revealed near total coverage on day 1 by cells cultured on the bioconjugated scaffolds, as well as their high degree of viability (green). Decreased confluence was observed over time; however, cells on the bioconjugated scaffolds demonstrated a higher retention rate relative to those on untreated controls.

3.4. HUVEC viability and adhesion

The results of viability assays and fluorescence imaging to evaluate cell morphology are shown in figure 4. Cells cultured on untreated scaffolds generally adhered near the edges of the scaffold and the premade indentations and did not appear to associate strongly with the scaffold surface (figures 3(B)–(I) and (D)–(I)). Additionally, we observed aggregates of cells adhering to each other rather than to the material, which appeared to become even more apparent over time (figures 4(D)–(I)–III). Similarly, the untreated scaffolds were characterized by a relatively high degree of nonviable cells, as well as low degree of scaffold surface coverage. By day 7, only sparse distributions of cells displaying a round morphology remained adhered to the scaffold. These observations

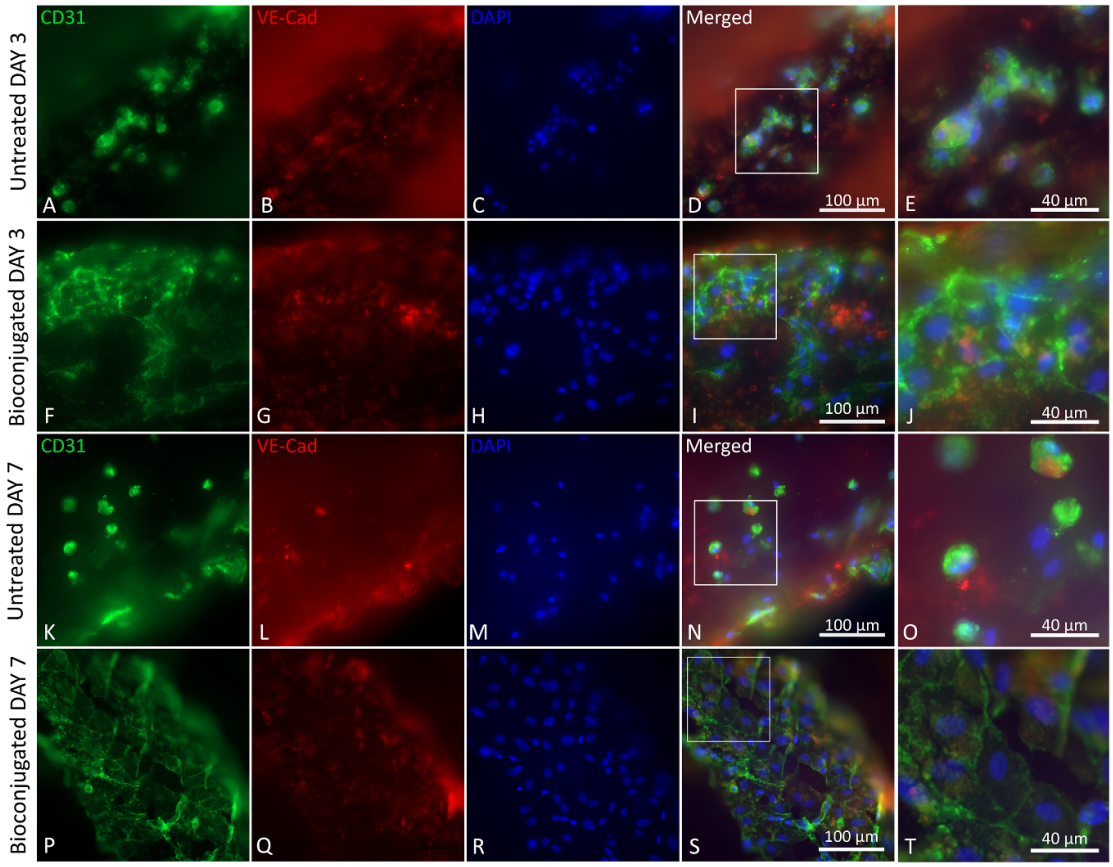

Figure 5. Immunofluorescence staining of HUVECs cultured on half-channel nanocellulose–alginate scaffolds. HUVECs were cultured on untreated nanocellulose–alginate scaffolds (A)–(E); (K)–(O) and laminin-conjugated scaffolds (F)–(J); (P)–(T). Staining was performed on days 3 (A)–(J) and 7 (K)–(T) post-seeding. Area of magnification is denoted by a white square to show cell–cell interactions. Cells were stained with the endothelial cell marker CD31 (green) and the tight junction marker VE-cadherin (VE-Cad; red) combined with DAPI for nuclear staining (blue).

confirmed the poor adhesive properties of nanocellulose, as described by Bodin *et al* [18].

By contrast, cells cultured on bioconjugated scaffolds formed nearly confluent layers of apparently viable cells that displayed a cobblestone morphology on culture day 1 (figures 4(A)–(I) and 5(C)–(I)). This near total confluence of the scaffold surface was not sustained over the course of the entire culture time and began to decline by day 3. On day 7, the majority of cells was located within the half-cylindrical indentations of the scaffold, with a fragmented cell layer also visible on the flat areas of the construct. Despite this time-dependent decrease in confluence, the numbers of viable cells remained higher relative to those on the control surfaces, where almost no cells remained adhered to the surface on the final day. Moreover, cells maintained an outstretched morphology and displayed tube formations (figures 4(A)–(I), (B-II), and (CI)), representing a cellular response to angiogenic signals present in the environment and a precursor to remodelling of the cell layer to form capillary-like structures [47]. These findings suggested that laminin bioconjugation to nanocellulose–alginate hydrogel scaffolds increased cell retention and viability for up to 1 week *in vitro* and elicited an angiogenic response from cells on the treated scaffolds.

Previous studies demonstrated the positive effects of similar types of bioconjugation on the adhesive properties of nanocellulose scaffolds. Zheng *et al* [20] observed an increased cell adhesion and proliferation on bacterial nanocellulose membranes bioconjugated with collagen using $NaIO_4$ oxidation. Additionally, Kuzmenko *et al* [21] demonstrated how covalent binding of fibronectin and collagen promotes endothelial cell attachment to cellulose surfaces. In contrast to our studies, both Wen and Kuzmenko used nanocellulose membranes whereas we used a 3D bioprintable nanocellulose–alginate hydrogel. In the present study, we demonstrated that laminin bioconjugation enhanced endothelial cell adhesion for up to 1 week *in vitro*. Moreover, despite an observed decrease in confluence, cell adhesion remained higher on bioconjugated scaffolds relative to untreated controls. The decrease in confluence is likely attributable to scaffold disintegration due to accelerated alginate degradation as a known consequence of partial alginate oxidation [42]. Furthermore, it is possible that this effect could be avoided by performing oxidative treatment prior to hydrogel preparation. Additionally, this

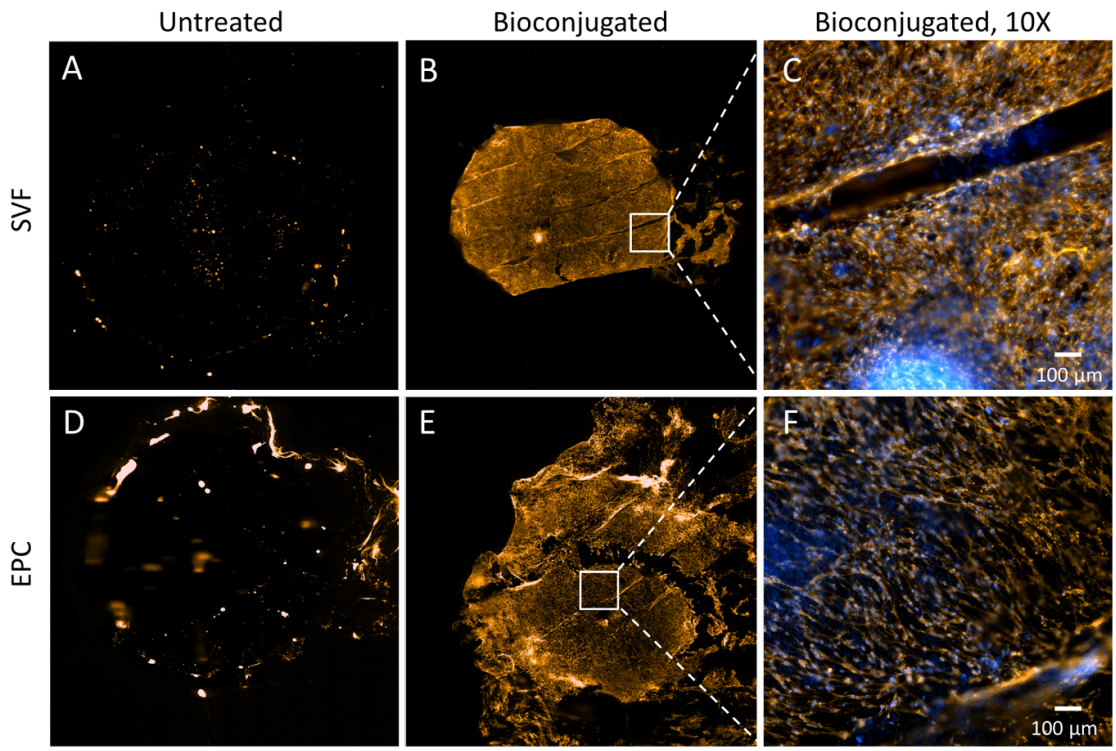

Figure 6. Surface coverage and morphology of adipose tissue-derived cell populations cultured on bioconjugated scaffolds. Confocal imaging of actin filaments (orange) to visualize overall cell-surface coverage of the SVF (A)–(C) and EPCs (D)–(F) on bioconjugated (B), (E) and untreated (A), (D) scaffolds. Areas marked with white squares are presented at 10× magnification (C), (F) to allow visualisation of cell morphology along with counterstained cell nuclei (blue). Analysis revealed near total cell coverage on bioconjugated scaffolds, whereas cells on control surfaces formed aggregates, indicating limited interaction with the scaffold.

may possibly mean that the effects of the bioconjugation with respect to increased cell adhesion might be retained for even longer periods of time. These findings showed that laminin bioconjugation enhanced cell adhesion, suggesting that optimizing this method might prolong the effects of this protocol on cell adhesion. Additionally, the nanocellulose–alginate hydrogel has suitable properties for 3D bioprinting, which further supports the potential for regenerative applications. The ability to both manipulate tissue architecture through 3D bioprinting as well as increasing the bioactivity of the material itself could possibly enhance vascularization in more physiological conditions.

Figure 5 shows immunofluorescence results targeting cells on bioconjugated and untreated scaffolds for 3 and 7 d in static culture. On day 3, some endothelial cells expressed CD31 in the bioconjugated group (figure 5(F)), whereas the control samples showed fewer attached cells with a rounder cell morphology and lower viability (figure 5(A)). The difference between groups was more pronounced on day 7, at which time larger endothelial layers in the half-channels exhibited stronger CD31 expression on the laminin-conjugated surfaces (figure 5(P)), whereas the controls showed few cells and no tight junctions (figure 5(K)). Despite that the overall VE-cadherin expression was observed to be low for both groups, there was still a noticeable higher level of expression on days 3 and 7 for the laminin-conjugated samples compared to the untreated samples. VE-cadherin expression is an important parameter that describes the status of cell–cell interactions, and previous studies report increases in VE-cadherin-mediated VE cell interactions in flow cultures as a result of mechanotransduction [48, 49]. These findings indicated that laminin bioconjugation promoted the expression of cell markers typically associated with healthy endothelium.

3.5. Viability, confocal imaging, and quantification of adipose tissue-derived cells

For both EPCs and the SVF seeded on bioconjugated scaffolds, we observed an overall high degree of viability on day 3 *in vitro*, which agreed with previous findings related to HUVEC-seeded scaffolds (figure S2). Confocal imaging on day 3 revealed a high level of confluence on the bioconjugated scaffolds along with near total coverage of cells (figure 6), which demonstrated an outstretched cobblestone-like morphology and no clear differences between cell types in terms of either morphology or confluence (figures 6(B), (C), (E), and (F)). By contrast, the untreated scaffolds showed low cell coverage and aggregates of densely packed cells rather than cells adhering to the scaffold (figures 6(A) and (D)). These findings agreed with previously described observations of HUVEC-coated scaffolds and confirmed that laminin bioconjugation

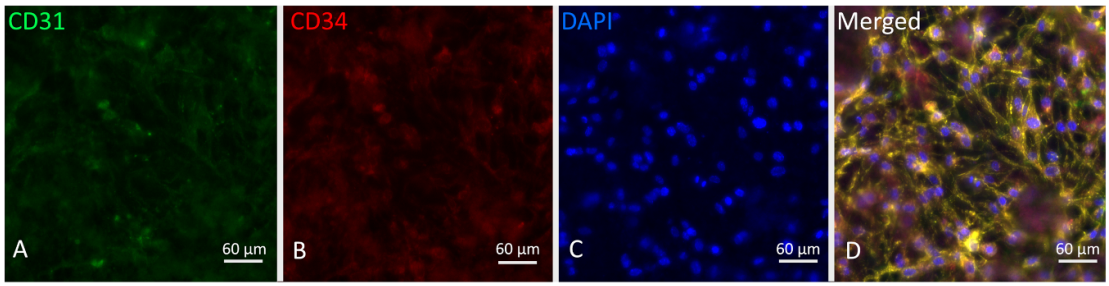

Figure 7. Immunofluorescence staining of CD31 and CD34 on EPCs cultured on bioconjugated scaffolds. Confocal images (20× magnification) showing staining of CD31 ((A); green), CD34 ((B); red), nuclei ((C); blue), and merged + actin filaments ((D); orange). Cells expressed both CD34 and CD31, indicating that EPCs differentiated into mature endothelial cells.

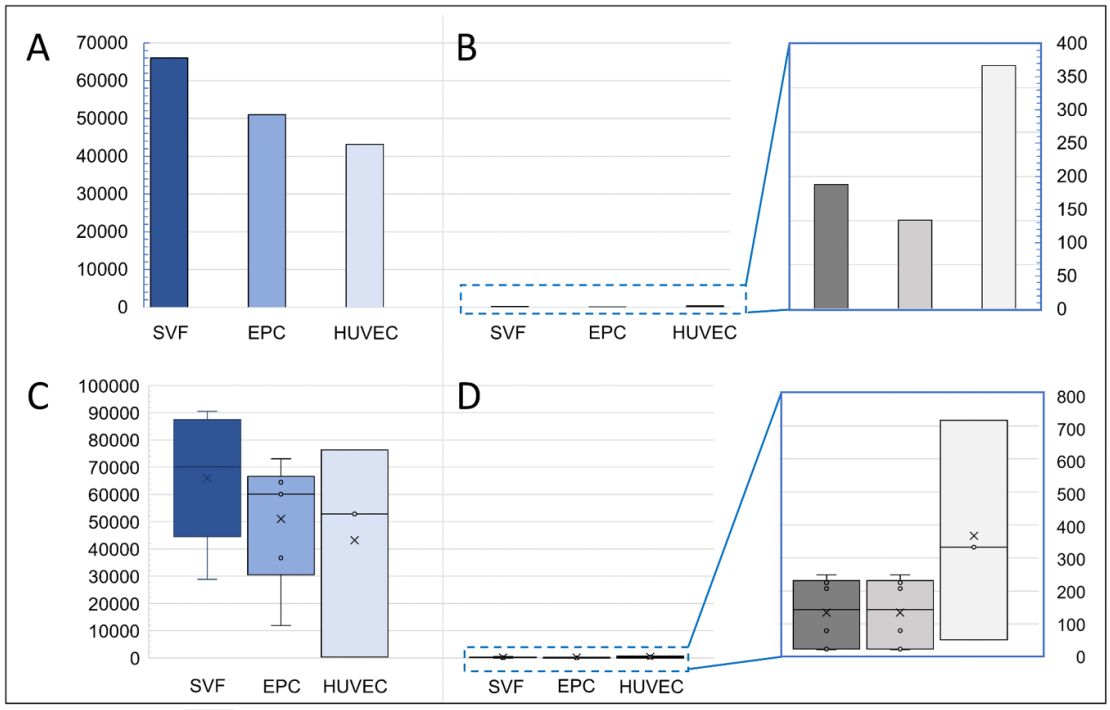

Figure 8. Cell density according to scaffold treatment and cell type. The bar graph (top) shows the average cell density (cell nuclei cm^{-2}) on bioconjugated (A) and untreated scaffolds (B). The average cell densities on the bioconjugated scaffolds coated with SVF, EPCs ($n = 6$) and HUVECs ($n = 3$) were 66 006, 51 077 and 43 192 cells cm^{-2}, respectively. The corresponding cell densities on the untreated controls were 188, 134 and 367 cells cm^{-2}. The box plot (bottom) shows the distribution of data points for bioconjugated (C) and untreated (D) scaffolds seeded with the SVF, EPCs, or HUVECs after 3 d of culture. For all cell types, bioconjugated scaffolds displayed a higher cell density relative to that on untreated scaffolds.

enhanced the adhesive properties of the scaffold for multiple cell types.

We identified positive immunofluorescence staining for CD34 and CD31 on EPCs present on bioconjugated scaffolds after 3 d of culture (figure 7). Given the importance of CD31 as a marker of mature endothelial cells, this result suggested that the EPCs had begun to differentiate, and that laminin bioconjugation promoted the differentiation of EPCs isolated from adipose tissue into mature endothelial cells. This is particularly promising for the pursuit of an autologous source of endothelial cells for tissue-engineering applications and vascularisation of biofabricated tissue grafts.

Figure 8 describes the differences in average cell density between the bioconjugated SVF-, EPC-, and HUVEC-laden scaffolds and untreated scaffolds. Kruskal–Wallis analysis revealed no significant difference in cell density between the bioconjugated and untreated scaffolds according to cell type, suggesting that the choice of cell type for seeding and *in vitro* culture did not affect cell adhesion regardless of treatment. Additionally, we confirmed a significant increase in cells density on the bioconjugated scaffolds relative to the untreated scaffolds, which supported the importance of the bioconjugation protocol.

The SVF is an important component of research targeting the *in vitro* creation of vascularized tissues

due to its diverse cell composition and ease of isolation. Additionally, its relevance within the field of regenerative medicine has been emphasized due to its native population of mesenchymal stem cells, which is significantly larger than that found in bone marrow and plays a major role in paracrine signalling in native adipose tissue through the secretion of growth factors, cytokines, and other signalling molecules [49]. Clinically, use of the SVF has been assessed for multiple applications, including wound healing, scar treatment, and various orthopaedic procedures [50]. Additionally, a previous report demonstrated the ability of the SVF to self-assemble into functional vasculature, which is partially attributable to the paracrine signalling of native immunoregulatory cells [26–29]. The present findings offer insight into additional applications of the SVF to harness its inherent vascularisation potential for endothelialisation by separating EPCs for *in vitro* expansion and subsequent seeding of nanocellulose-based scaffolds for tissue engineering. Given the ease with which the SVF can be isolated via standard liposuction and large volumetric tissue yields, these characteristics support the relevance of adipose tissue as an autologous cell source for generating a vascularized tissue graft *in vitro*.

4. Conclusions

In summary, we functionalised nanocellulose hydrogel scaffolds via laminin bioconjugation to promote the adhesion of cells sourced from adipose tissue. *In vitro* studies confirmed significant elevations in the viability and confluence of cells cultured on the bioconjugated scaffolds, as well as maturation of SVF-derived $CD34^+$ EPCs into $CD31^+$ endothelial cells. These findings demonstrated the utility of laminin bioconjugation to support cells isolated from the SVF of adipose tissue and suggest this as a viable strategy for generating autologously endothelialised scaffolds. Furthermore, the results promote the development of fully vascularized scaffolds for tissue-engineering applications.

Data availability statements

The data cannot be made publicly available upon publication because they are not available in a format that is sufficiently accessible or reusable by other researchers. The data that support the findings of this study are available upon reasonable request from the authors.

Acknowledgments

We acknowledge the Centre for Cellular Imaging at the University of Gothenburg and the National Microscopy Infrastructure, NMI (VR-RFI 2016-00968) for aiding with microscopy. The authors would also like to thank Professor John S Fletcher at Gothenburg University for assisting in ToF-SIMS analysis. We would also like to acknowledge the help received from Jason Fye, MS, PhD, with English language editing.

Fundings

This work was financed by The Swedish Research Council (VR) 2021-0097, the IngaBritt and Arne Lundberg Research Foundation (LU2020-0016, LU2018-0031), and by Grants from the Swedish State under the agreement between the government and the county councils, the ALF-agreement (ALFGBG-716621; ALFGBG-971618). Furthermore, this study was supported by Grants from the Göteborg Medical Society, the Mary von Sydow Foundation, and the Magnus Bergvalls Foundation. Research Council of Norway is greatly acknowledged for funding of the project 3D TUNINK and TUNIGUIDE. The funders of the study played no role in study design; data collection, analysis, and interpretation; the writing of the report; or in the decision to submit the article for publication.

Conflict of interest

The authors declare that they have no competing financial interests.

ORCID iDs

Kristin Oskarsdotter https://orcid.org/0000-0002-8531-3182
Stina Simonsson https://orcid.org/0000-0001-9020-3714

References

[1] Basu A, Lindh J, Ålander E, Strømme M and Ferraz N 2017 On the use of ion-crosslinked nanocellulose hydrogels for wound healing solutions: physicochemical properties and application-oriented biocompatibility studies *Carbohydrate Polym.* **174** 299–308
[2] Habibi Y 2014 Key advances in the chemical modification of nanocelluloses *Chem. Soc. Rev.* **43** 1519–42
[3] Martin C and Jean B 2014 Nanocellulose/polymer multilayered thin films: tunable architectures towards tailored physical properties *Nord. Pulp Pap.Res. J.* **29** 19–30
[4] McKee J R, Hietala S, Seitsonen J, Laine J, Kontturi E and Ikkala O 2014 Thermoresponsive nanocellulose hydrogels with tunable mechanical properties *ACS Macro Lett.* **3** 266–70
[5] Siqueira P, Siqueira É, De Lima A E, Siqueira G, Pinzón-Garcia A D, Lopes A P, Segura M E C, Isaac A, Pereira F V and Botaro V R 2019 Three-dimensional stable alginate-nanocellulose gels for biomedical applications: towards tunable mechanical properties and cell growing *Nanomaterials* **9** 78
[6] Xu C *et al* 2018 3D printing of nanocellulose hydrogel scaffolds with tunable mechanical strength towards wound healing application *J. Mater. Chem.* B **6** 7066–75
[7] Apelgren P, Sämfors S, Säljö K, Mölne J, Gatenholm P, Troedsson C, Thompson E M and Kölby L 2022 Biomaterial

and biocompatibility evaluation of tunicate nanocellulose for tissue engineering *Biomater. Adv.* **137** 212828
[8] Markstedt K, Mantas A, Tournier I, Martínez Ávila H, Hägg D and Gatenholm P 2015 3D bioprinting human chondrocytes with nanocellulose-alginate bioink for cartilage tissue engineering applications *Biomacromolecules* **16** 1489–96
[9] Hickey R J and Pelling A E 2019 Cellulose biomaterials for tissue engineering *Front. Bioeng. Biotechnol.* **7** 45
[10] Bacakova L, Pajorova J, Bacakova M, Skogberg A, Kallio P, Kolarova K and Svorcik V 2019 Versatile application of nanocellulose: from industry to skin tissue engineering and wound healing *Nanomaterials* **9** 164
[11] Wang Q, Sun J, Yao Q, Ji C, Liu J and Zhu Q 2018 3D printing with cellulose materials *Cellulose* **25** 4275–301
[12] Siqueira G, Kokkinis D, Libanori R, Hausmann M K, Gladman A S, Neels A, Tingaut P, Zimmermann T, Lewis J A and Studart A R 2017 Cellulose nanocrystal inks for 3D printing of textured cellular architectures *Adv. Funct. Mater.* **27** 1604619
[13] Dai L, Cheng T, Duan C, Zhao W, Zhang W, Zou X, Aspler J and Ni Y 2019 3D printing using plant-derived cellulose and its derivatives: a review *Carbohydrate Polym.* **203** 71–86
[14] Jessop Z M, Al-Sabah A, Gao N, Kyle S, Thomas B, Badiei N, Hawkins K and Whitaker I S 2019 Printability of pulp derived crystal, fibril and blend nanocellulose-alginate bioinks for extrusion 3D bioprinting *Biofabrication* **11** 045006
[15] Heggset E B, Strand B L, Sundby K W, Simon S, Chinga-Carrasco G and Syverud K 2019 Viscoelastic properties of nanocellulose based inks for 3D printing and mechanical properties of CNF/alginate biocomposite gels *Cellulose* **26** 581–95
[16] Wu Y, Lin Z Y (William), Wenger A C, Tam K C and Tang X 2018 3D bioprinting of liver-mimetic construct with alginate/cellulose nanocrystal hybrid bioink *Bioprinting* **9** 1–6
[17] Helenius G, Bäckdahl H, Bodin A, Nannmark U, Gatenholm P and Risberg B 2006 *In vivo* biocompatibility of bacterial cellulose *J. Biomed. Mater. Res.* A **76** 431–8
[18] Bodin A, Ahrenstedt L, Fink H, Brumer H, Risberg B and Gatenholm P 2007 Modification of nanocellulose with a xyloglucan–RGD conjugate enhances adhesion and proliferation of endothelial cells: implications for tissue engineering *Biomacromolecules* **8** 3697–704
[19] Courtenay J, Sharma R and Scott J 2018 Recent advances in modified cellulose for tissue culture applications *Molecules* **23** 654
[20] Zheng Y, Wen X, Wu J, Wang L-N, Yuan Z, Peng J and Meng H 2015 Immobilization of collagen peptide on dialdehyde bacterial cellulose nanofibers via covalent bonds for tissue engineering and regeneration *Int. J. Nanomed.* **10** 4623
[21] Kuzmenko V, Sämfors S, Hägg D and Gatenholm P 2013 Universal method for protein bioconjugation with nanocellulose scaffolds for increased cell adhesion *Mater. Sci. Eng.* C **33** 4599–607
[22] Osorio M, Ortiz I, Gañán P, Naranjo T, Zuluaga R, van Kooten T G and Castro C 2019 Novel surface modification of three-dimensional bacterial nanocellulose with cell-derived adhesion proteins for soft tissue engineering *Mater. Sci. Eng.* C **100** 697–705
[23] Williams S K, Kleinert L B and Patula-Steinbrenner V 2011 Accelerated neovascularization and endothelialization of vascular grafts promoted by covalently bound laminin type 1 *J. Biomed. Mater. Res.* A **99A** 67–73
[24] Anderson D E J, Truong K P, Hagen M W, Yim E K F and Hinds M T 2019 Biomimetic modification of poly(vinyl alcohol): encouraging endothelialization and preventing thrombosis with antiplatelet monotherapy *Acta Biomater.* **86** 291–9
[25] Yu C, Guan G, Glas S, Wang L, Li Z and Turng L-S 2021 A biomimetic basement membrane consisted of hybrid aligned nanofibers and microfibers with immobilized collagen IV and laminin for rapid endothelialization *Bio-Des. Manuf.* **4** 171–89
[26] Heath C A 2000 Cells for tissue engineering *Trends Biotechnol.* **18** 17–19
[27] Bora P and Majumdar A S 2017 Adipose tissue-derived stromal vascular fraction in regenerative medicine: a brief review on biology and translation *Stem. Cell Res. Ther.* **8** 1–10
[28] Ramakrishnan V M and Boyd N L 2018 The adipose stromal vascular fraction as a complex cellular source for tissue engineering applications *Tissue Eng.* B **24** 289–99
[29] Säljö K, Apelgren P, Stridh Orrhult L, Li S, Amoroso M, Gatenholm P and Kölby L 2022 Long-term *in vivo* survival of 3D-bioprinted human lipoaspirate-derived adipose tissue: proteomic signature and cellular content *Adipocyte* **11** 34–46
[30] Koh Y J *et al* 2011 Stromal vascular fraction from adipose tissue forms profound vascular network through the dynamic reassembly of blood endothelial cells *Arterioscler. Thromb. Vascular Biol.* **31** 1141–50
[31] Callens S J P, Uyttendaele R J C, Fratila-Apachitei L E and Zadpoor A A 2020 Substrate curvature as a cue to guide spatiotemporal cell and tissue organization *Biomaterials* **232** 119739
[32] Fletcher J S, Rabbani S, Henderson A, Blenkinsopp P, Thompson S P, Lockyer N P and Vickerman J C 2008 A new dynamic in mass spectral imaging of single biological cells *Anal. Chem.* **80** 9058–64
[33] Hill R, Blenkinsopp P, Thompson S, Vickerman J and Fletcher J S 2011 A new time-of-flight SIMS instrument for 3D imaging and analysis *Surf. Interface Anal.* **43** 506–9
[34] Perkins D N, Pappin D J C, Creasy D M and Cottrell J S 1999 Probability-based protein identification by searching sequence databases using mass spectrometry data *Electrophoresis* **20** 3551–67
[35] Dado D and Levenberg S 2009 Cell–scaffold mechanical interplay within engineered tissue *Semin. Cell Dev. Biol.* **20** 656–64
[36] Saito T, Shibata I, Isogai A, Suguri N and Sumikawa N 2005 Distribution of carboxylate groups introduced into cotton linters by the TEMPO-mediated oxidation *Carbohydrate Polym.* **61** 414–9
[37] Röhrling J, Potthast A, Rosenau T, Lange T, Ebner G, Sixta H and Kosma P 2002 A novel method for the determination of carbonyl groups in cellulosics by fluorescence labeling. 1 Method development *Biomacromolecules* **3** 959–68
[38] Kristiansen K A, Potthast A and Christensen B E 2010 Periodate oxidation of polysaccharides for modification of chemical and physical properties *Carbohydrate Res.* **345** 1264–71
[39] Isobe N, Lee D-S, Kwon Y-J, Kimura S, Kuga S, Wada M and Kim U-J 2011 Immobilization of protein on cellulose hydrogel *Cellulose* **18** 1251–6
[40] Errokh A, Magnin A, Putaux J-L and Boufi S 2018 Morphology of the nanocellulose produced by periodate oxidation and reductive treatment of cellulose fibers *Cellulose* **25** 3899–911
[41] Nikolic T, Kostic M, Praskalo J, Pejic B, Petronijevic Z and Skundric P 2010 Sodium periodate oxidized cotton yarn as carrier for immobilization of trypsin *Carbohydrate Polym.* **82** 976–81
[42] Bouhadir K H, Lee K Y, Alsberg E, Damm K L, Anderson K W and Mooney D J 2001 Degradation of partially oxidized alginate and its potential application for tissue engineering *Biotechnol. Prog.* **17** 945–50
[43] Li J, Wan Y, Li L, Liang H and Wang J 2009 Preparation and characterization of 2,3-dialdehyde bacterial cellulose for potential biodegradable tissue engineering scaffolds *Mater. Sci. Eng.* C **29** 1635–42
[44] Grant D S, Tashiro K-I, Segui-Real B, Yamada Y, Martin G R and Kleinman H K 1989 Two different laminin domains

mediate the differentiation of human endothelial cells into capillary-like structures *in vitro Cell* **58** 933–43
[45] Kim S, Bell K, Mousa S A and Varner J A 2000 Regulation of angiogenesis *in vivo* by ligation of integrin α5β1 with the central cell-binding domain of fibronectin *Am. J. Pathol.* **156** 1345–62
[46] Pietrucha K, Marzec E and Kudzin M 2016 Pore structure and dielectric behaviour of the 3D collagen-DAC scaffolds designed for nerve tissue repair *Int. J. Biol. Macromol.* **92** 1298–306
[47] Matsui J, Wakabayashi T, Asada M, Yoshimatsu K and Okada M 2004 Stem cell factor/c-kit signaling promotes the survival, migration, and capillary tube formation of human umbilical vein endothelial cells *J. Biol. Chem.* **279** 18600–7
[48] Vestweber D 2008 VE-cadherin: the major endothelial adhesion molecule controlling cellular junctions and blood vessel formation *Arterioscler. Thromb. Vascular Biol.* **28** 223–32
[49] Rabodzey A, Yao Y, Luscinskas F W, Shaw S K and Dewey C F 2007 Early response of endothelial cells to flow is mediated by VE-cadherin *Cell Commun. Adhes.* **14** 195–209
[50] Andia I, Maffulli N and Burgos-Alonso N 2019 Stromal vascular fraction technologies and clinical applications *Expert Opin. Biol. Ther.* **19** 1289–305